RESEARCH ARTICLE

Machining millimeter-scale deep holes in SiC$_f$/SiC material using femtosecond laser filamentation effect

Jie Zhao[1,2], Wenjun Wang[1,2*], Ruijia Wang[1,2], Jianlei Cui[1,2*]

[1] State Key Laboratory for Manufacturing System Engineering, Xi'an Jiaotong University, Xi'an 710054, China

[2] Shaanxi Key Laboratory of Intelligent Robots, Xi'an Jiaotong University, Xi'an 710054, China

Abstract: A 3.5 mm thick SiC$_f$/SiC material was drilled in air environment using a femtosecond laser filament effect. The surface morphology of deep micropores was observed by scanning electron microscopy and the depth and profile of the pores were observed using μm-CT. The variation of entrance diameter, exit diameter and depth variation with laser focus position and processing time was further analyzed. The results showed that as the processing time of femtosecond laser increases, the ablation threshold of the material reached saturation. The exit and entrance diameter also stopped increasing and the aperture tend to saturate. The focus entered the interior of the material, allowing the location of the peak power near the surface of the material. So the entrance aperture was of good quality and the exit aperture was round.

Keywords: laser technology; femtosecond laser filamentation effect; deep hole taper; aperture

1. Introduction

SiC$_f$/SiC material was a new strategic grade material with excellent properties such as high temperature resistance, low density, high specific strength, high specific mode, oxidation resistance and ablation resistance[1–3]. It has the potential to replace metals as a new generation of high temperature structural materials. It has been widely used in the fields of spacecraft thermal protection components, aero-engine hot end components and thermonuclear fusion shields.

In the field of aero-engine applications, in order to improve the processing life of materials, it was necessary to process the film cooling holes on engine accessories made of SiC$_f$/SiC material[4–6]. The traditional punching process could not meet the requirements of deep micro-hole processing for key parts of many high-precision products, thus greatly reducing the processing quality of the products[7–12]. The laser drilling technology has the advantages of high precision, high repeatability, low cost and low material consumption and played an increasingly important role in the modern manufacturing field. At present, the most processing method for laser processing of SiC$_f$/SiC materials was the use of ultrashort pulse lasers—high-frequency, low-pulse processing energy femtosecond laser processing materials. However, this kind of laser processing also has a certain thermal effect. The recasting material was prone to occur during the processing and the shape of the hole was easy to bend. When machining materials with high single-pulse energy and low-repetition femtosecond laser, the processing heat effect was small[13]. At the same time, it was also found that the bending of the hole shape was reduced. High single-pulse energy, low-repetition femtosecond lasers could produce bright plasma channels and transmit over long distances when transporting in air. Bright plasmas were also known as laser filaments[14].

In this paper, the deep micropore processing of SiC$_f$/SiC materials was carried out by using the filament forming effect of femtosecond laser. The variation of the pore size, roundness and taper of the small hole with the average laser power and processing time was observed and recorded. The aperture size, roundness and depth of the holes with the

focus position and processing time were observed and recorded. The millimeter-scale deep holes prepared by femtosecond laser filaments could be applied to practical engineering fields.

2. Experimental principle

Femtosecond laser filament formation was formed by an optical lens focusing system. When the femtosecond laser was propagating in the air, the peak power of the femtosecond laser exceeded the critical power P_{cr} that enabled the ionization of the air, which caused the air to break down and thereby produced a white visible light. This phenomenon was the phenomenon of light filament[15–16].

This phenomenon was caused by the laser filamentation effect, which was a combination of the Kerr self-focusing effect and the plasma defocusing effect[17–20]. When the two reached dynamic equilibrium, the femtosecond laser could form a stable plasma channel in the air. The use of low-repetition, high-single-pulse energy femtosecond lasers for drilling was the use of the femtosecond laser filamentation effect for deep micro-holes processing.

Femtosecond laser filaments had the advantages of high ablation intensity, good uniformity and long propagation distance. Therefore, the femtosecond laser forming technology was used to replace the traditional focusing punching technology, and the conventional focusing punching technique used a tracking method[21].The focused laser spot always needs to track the top of the hole. When the trajectory of the laser spot was bent, the processing quality was greatly reduced. The low-repetition, high-single-pulse energy femtosecond lasers forming method could be used to form holes at one time, avoiding the defects of the conventional method.

3. Experimental

3.1 SiC$_f$/SiC fabrication

It has been shown that the relatively straight and independent fibers that are achieved through tow coating and unidirectional tape prepregging improve the effectiveness of the fiber for providing toughness and strength relative to systems using woven or braided reinforcement[22].This overall fabrication process is shown schematically in **Figure 1.** The surface roughness of the SiC$_f$/SiC composites was about Ra6.0, and the density was above 2.5 g/cm^3. Before being laser machined, the specimens were cleaned with alcohol in an ultrasonic bath for 30 min. The size of the samples is $20 \times 5 \times 3.5$ mm^3.
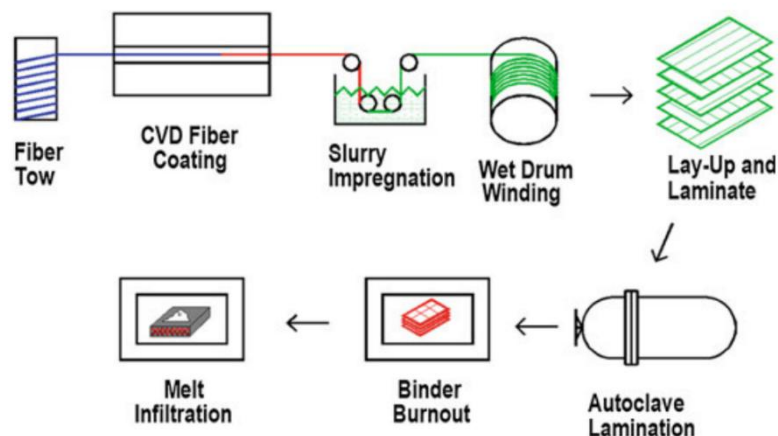

Figure 1. Schematic representation MI CMC fabrication process[22]

3.2 Laser machining procedure

The experimental equipment for laser drilling is shown in **Figure 2.** The laser source was employed with ultrashort visible (800nm) light pulses from the ultrafast laser system. It delivered the average power in the range of 1–4W at a repetition rate of 1000Hz with a nominal pulse duration of 150fs. The laser pulses process a Gaussian spatial energy distribution. The pulse energy was adjusted to a constant value of 4.0 mJ using variable neutral density filters. The

laser beam, about 26μm diameter, was focused onto the samples surface using an convex lens of 200 mm focal length. The femtosecond laser was focused into a filament through a 200mm lens to form a relatively stable filament channel in the air. The diameter of drilling holes was set at 500μm. To achieve through-thickness hole drilling, the machining stage moved in a circular manner along the Z processing axial. In experiments, the samples were placed on the computer-controlled ufab stage including three linear stages. In order to obtain a higher quality round hole, the processing method adopted is a ring cutting process. The method adopted in this experiment is to rotate the ufab platform, and the workpiece is fixed on the ufab platform, as shown in Figure 3a, while the femtosecond laser beam does not move. The maximum speed that can be achieved with the ufab platform is 300 μm/s. The material to be processed rotates with the ufab platform, the rotating axis of the workpiece deviates from the processing optical axis. The rotating ufab platform causes the laser to form a series of circumferential contours on the surface of the workpiece, and the material is removed layer by layer. Finally, a small hole having a certain radius is formed, and the scanning track is as shown in Figure 3b. Each cycle has a certain amount of material removed, repeated several cycles, and a certain amount of material is removed to form a hole.
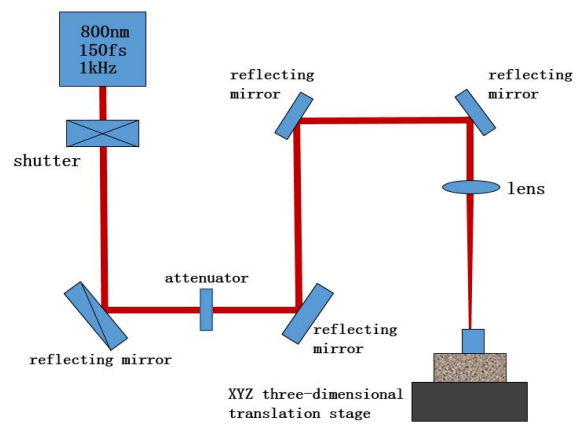

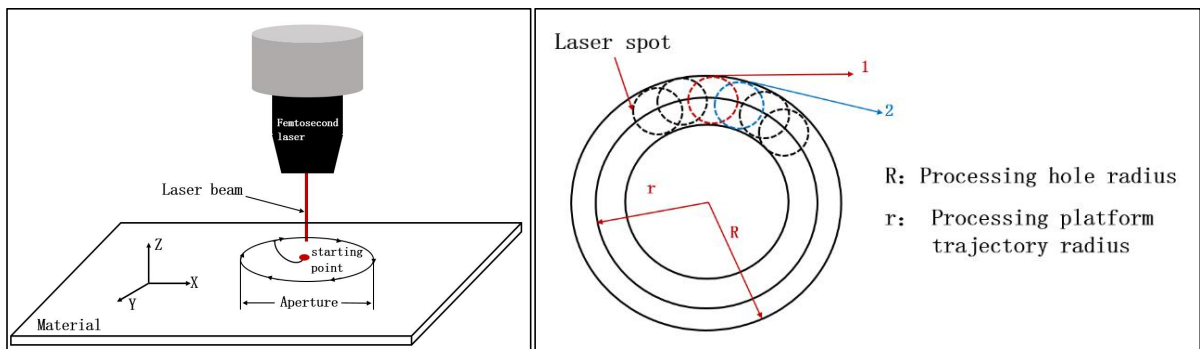**Figure 2.** Experimental apparatus for preparing deep holes by femtosecond laser filament formation

Figure 3a   **Figure 3**b

Figure 3. Processing schematic

In the first set of experiments, the dependence of drilling holes on the number of processing time studied. Then the second set of experiments with the focus position of the laser beam relative to the sample surface along the processing z-axial direction was investigated. Hereafter, focus position is indicated as "0 focus" when the focus is on the surface, as "-1.0 focus" when the focus is -1.0mm below the surface. All the machining processes were carried out under the temperature of 18–20∘C with the room humidity of 50–70% in air atmosphere.

4. Results and discussion

4.1 Effect of processing time

The femtosecond laser filament acted on the SiC$_f$/SiC material with a single pulse energy of 4 mJ, a workpiece rotation speed of 300 μm/s, -3 mm focus, and a processing time of 15 seconds within 1 minute. After more than 1 minute, the interval was set as 30 seconds. The processing time was 30s, 45s, 60s, 90s, 120s, 150s and 180s. The material inlet aperture of 3.5mm thick was shown in **Figure 4**
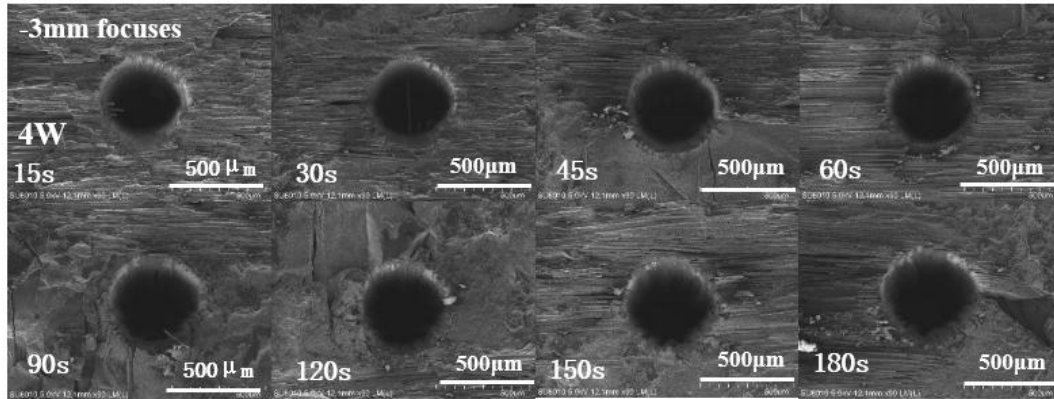

Figure 4. The entrances of these holes variation with processing time

During the interaction between the laser and the material, as the processing time increased, the entrances of these holes drilled by laser would tend to be saturated. When the laser ablated material, the ablation threshold of the material increased with the number of pulses, and the ablation threshold gradually decreased. The ablation threshold reached saturation. The energy distribution of the laser follows a Gaussian distribution. When the laser energy density is lower than the ablation threshold, the material does not undergo further ablation, as shown in **Figure 5.** When the focus spot of the pulsed laser is scanned along the motion trajectory, multiple pulses affect the illumination point of the scan path.
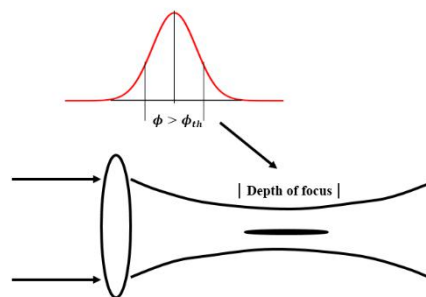

Figure 5. Removing material area distribution after focusing

The effect of measuring the multi-pulse effect of the scan ablation is the number of effective pulses that were irradiated by a fixed position on the scan line. It could be seen from the **Figure 3** that the effective pulse number calculated by irradiating the fixed position along the scanning center was $N = \dfrac{d}{s/f}$.
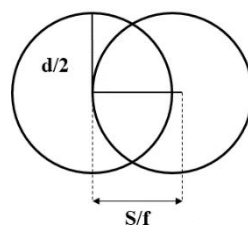

Figure 6. Schematic diagram of the relative position and microstructure

width variation of adjacent pulses in scanning processing

d: spot diameter at the focus, s: scan line speed, f: laser re-frequency. The parameters selected in the experimental

conditions were calculated, and the effective pulse number was N=400. When the cumulative effect of multi-pulse ablation reduced the ablation threshold of the material to the ablation threshold corresponding to 400 pulses, the laser energy density at the edge of the hole could not exceed the ablation threshold corresponding to 400 pulses. The prolonged processing time did not increase the effective number of pulses at a fixed position. The prolonged processing time did not cause the entrances of these holes diameter increase and the entrances of these holes tends to be saturated. It could be seen from **Figure 5** that the energy density of the peak power position was the largest. Because of the depth of focus, the energy density of the beam within a certain length was greater than the damage threshold, so that the material removed region is approximately a cylindrical shape. The greater the energy density was, the lower the radius of the removed area was. So the tapered shape was formed.

As the processing time increased, the depth of the hole increased significantly. When the processing time was 15s, the exit of these holes of the material was not acquired, and the hole shape has a distinct taper. When the laser energy was transmitted from the surface into the hole, and the material was removed by multiple irradiations. As the depth increased, the laser energy gradually decreased and the area of the energy density greater than the damage threshold also decreased. So the area where the material was removed was smaller and also formed a tapered hole.

When the processing time continued to be increased, the bottom exit of the material appeared at a processing time of 30s and a bend occurred at the bottom of the hole. However, as the processing time continues to increase, the laser transmission was corrected by the filament and the hole was corrected to a straight hole when processed to 45s. As time continued to be increased, the shape of the hole was a straight hole, but they were all tapered, as shown in **Figure 7.**
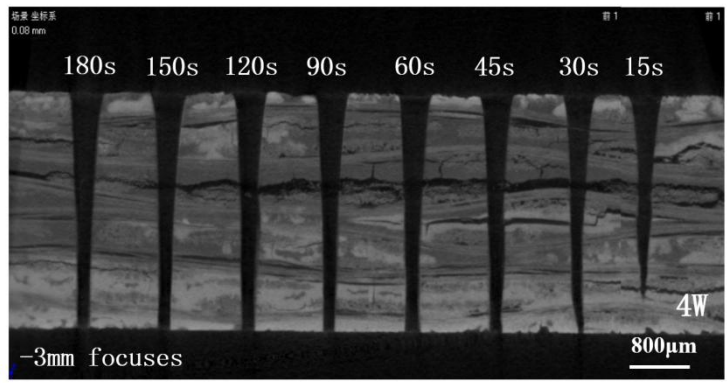

Figure 7. Holes depth as a function of processing time

Figure 8 shows the effect of different processing times for different micromachining exit of holes by -3mm focus. There would be periodical saturation of the exit aperture during a certain processing time. After further processing, the exit aperture would continued to increase until the final saturation is reached. The exit aperture was in staged saturation at processing times of 45s, 60s, and 90s. The exit aperture was at final saturation at processing times of 120s, 150s and 180s.
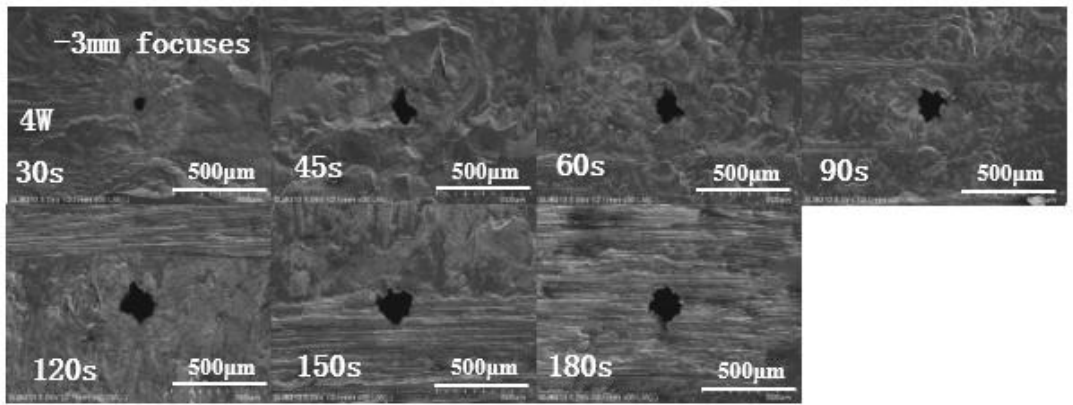

Figure 8. Exit aperture variation with processing time

As the processing time increased, the entrances of these holes diameter reached saturation, and the outlet pore size continued to increase until the exits of these holes diameter was saturated. From the above analysis, the processing of the holes type was tapered.

In the early stage of laser processing materials, laser energy could all act on the surface of the material due to the shallow holes. With the processing time extended, the depth of the hole was increased. The laser was diffracted at the entrance, reducing the energy of the laser entering the interior of the material. At the same time, the laser was refracted and reflected on the sidewall of the holes so that the energy of the laser reaching the bottom of the material was further reduced, and the diameter of the exits was further reduced. When the entrances was processed for 15s, the diameter of the entrances has been processed to 500 μm, and the exit occurred when processing for 30s. As time increased, the processed material could be ejected from the bottom exit of the holes, reducing the build-up of material inside the hole. As the bottom of the material continued to interact with the peak power of the laser, the peak power was above the ablation threshold of the material, causing an increase in the diameter of the exit. The uneven distribution of the material inside would result in different materials being removed. Therefore, the exit aperture would have periodical saturation. When the processing time reached 120s, the ablation threshold of the edge of the exit aperture was higher than the laser energy density, which caused the exit aperture not to continue to increase and to reach final saturation.

4.2 Effect of focus position

The relative position of the laser geometric focus to the surface of the material affected the quality of the process. The distance of the geometric focus from the surface of the material was defined as the amount of defocus. Focus position was indicated as "0 focus". The focus was on the surface, as "+ X mm focus" when the focus was X mm above the surface. The focus was below the surface, as "- X mm focus" when the focus was X mm below the surface.

The single pulse energy was 4mJ. The workpiece rotation speed was 300μm/s. The processing time was 60s. The focus position was 0 --6mm focus as shown in **Figure 9.**
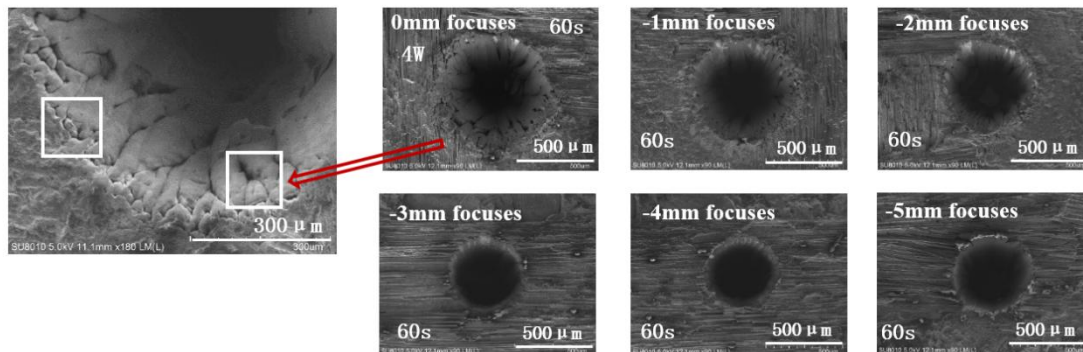

Figure 9. Influence of different defocusing amount on inlet aperture

When the focus position was 0 focus,-1mm focus and -2mm focus, the inlet aperture was relatively large and the inlet roundness were poor. Many gullies could be clearly seen at the entrance hole. The energy was diverged relatively large, resulting in a large entrance aperture. A part of the energy was diverged to the periphery, resulting in a small filament formed around the periphery, and the energy density of the small filament was relatively high. At the same time, the peripheral material could be etched by the small filament, and the small filament continued to process the material to form a gully[23]. The energy distribution was mainly the plasma defocusing effect, the Kerr self-focusing effect is reduced. The boundary material was irradiated with the energy of the laser, and material modification occurred around the orifice.

When the focus position was -3mm focus, -4mm focus and -5mm focus, the number of gullies was reduced. The quality of the entrance of the hole was getting better. The modified portion around the orifice was much reduced, as shown in **Figure 9.** In the propagation region of this part of the laser, the energy distribution was mainly the Kerr self-focusing effect, and the plasma defocusing effect is reduced.

In the process of spatial propagation of laser light, the energy was mainly concentrated, and no divergence occurred, resulting in high roundness of the type. When the focus position was -2mm focus,-3mm focus, -4mm focus, -5mm focus, and -6mm focus, the exit diameter was shown in **Figure 10.** The exit diameter with -2 mm focus and -3 mm focus was smaller than the exit diameter of -4 mm focus and -5 mm focus. The exit diameter of -4 mm, -5 mm was the largest, and the maximum diameter of the exit was 220 μm.
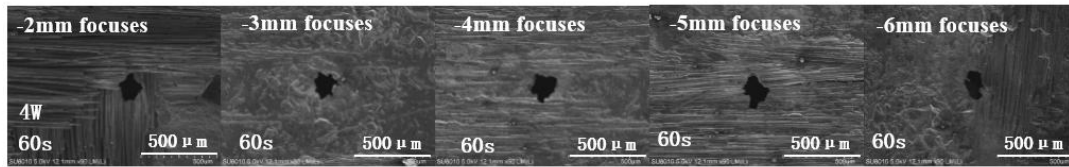

Figure 10. Influence of different defocusing amount on outlet pore diameter

In terms of depth, the shape of the hole first formed a taper when the focus position was -0mm focus and -1 mm focus. As the negative defocusing amount of the processing increased, the tapered holes gradually extended into the interior of the material and the material was machined into through holes. When the focus position was -2mm focus,-3mm focus, -4mm focus, -5mm focus, and -6mm focus, the material was processed into a through hole as shown in **Figure 11.**
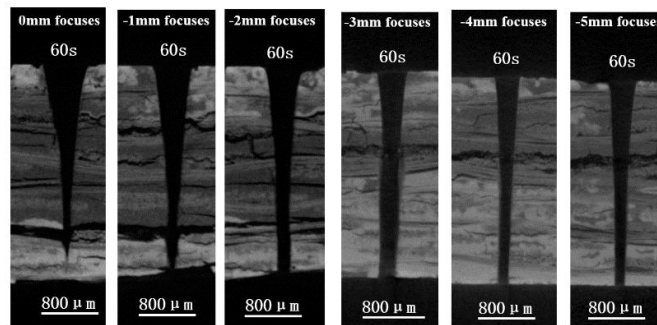

Figure 11. Influence of different defocusing amount on pore structure

The simulation of the laser energy distribution along the propagation direction of the single pulse energy of 4 mJ showed that the peak power of the femtosecond laser was shifted away from the geometric focus and moved toward the incident direction of the laser, as shown in **Figure 12.** This was because the peak power of the laser incident was greater than the critical power P_{cr} at which the filament effect occurs, resulted from Kerr self-focusing and plasma defocusing, causing the peak power to move toward the incident direction of the laser. It was found by experiments that the exit pore size of the micropores reached the maximum when the focus position was -4mm focus and -5mm focus. This meant that the peak power was shifted to a position when the focus position was between -3 mm focus, -4mm focus, and -5mm focus. When the laser energy propagates to the bottom of the hole, more laser energy was transmitted to the bottom of the hole. The energy density exceeded the material ablation threshold at the edge of the exit aperture, causing the exit diameter to increase. When the laser propagated to the focus position of 0mm focus, -1mm focus, and -2mm focus, the energy has been lost. At the same time the filament was split into small filaments, and the energy was dispersed. This indicated that the energy reaching the bottom of the material was reduced, the energy density at the edge of the exit orifice was below the material ablation threshold, which caused the diameter of the exit to decrease, and even the exit aperture could not be machined.
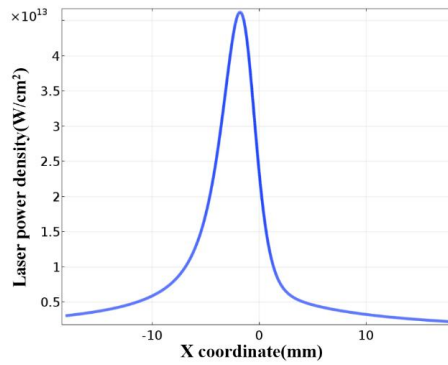
Figure 12. 4W laser energy density distribution along the laser propagation direction

The shortest time for laser processing of the material was recorded and the results were shown in **Figure 13.** At the position of the geometric focus, the SiCf/SiC material could not be processed into through holes, and the processing depth tended to be saturated. At the focus position of -1mm focus the laser processed material was used for 3 minutes until the exit of the material appeared. At the focus position of -2mm focus, the time required for the bottom exit of the material to be processed was reduced.

At this time, the peak power of the energy was not at the position of the geometric focus, moving toward the lens, at the position of negative defocus. At the focus position of -5mm focus to -2mm focus, a 3.5 mm thick SiC$_f$/SiC material was processed. The corresponding peak power intensity has little change in energy in the direction of laser propagation. The higher the peak power, the shorter the processing time of the material was need, which meant that the ablation rate of the laser material is higher.At the focus position of -3mm focus processing of 3.5 mm thick material required the shortest processing time, only 32s. This also means that the optical filament here has the greatest ablation rate at the focus position of -3mm focus. The processing time at the focus position of -2mm focus and -4mm focus were 36s and 44s.The processing time was also relatively short, indicating that the ablation rate was also high at the focus position of -2mm focus and -4mm focus. The position produced by the filament effect was the starting point of the filament. If the laser was ionized at the position in front of the material, the ionization caused a nonlinear loss of energy. Therefore, choosing the best machining position was to place the material before ionization occurs. However, the distribution of energy was also a Gaussian distribution.

It did not mean that at the starting point of ionization, it was the maximum position of energy. The peak power was far from the geometric focus, and the most suitable position for the material to be processed was different for each material.

5. Conclusions

The above experiments respectively showed the effects of different laser defocusing amounts and different processing times on the processing of deep micro-holes. Experiments had shown that the focus moved toward the inside of the material and the entrance diameter of the hole decreased firstly. At the focus position of -3mm focus and -4mm focus, the entrance diameter was the smallest and the processing quality was the best. As the focus moved toward the inside of the material more deeply, the entrance diameter would become larger. The exit diameter would increase with the increase of the focus moving the inside of the material. The exit diameter would be the largest at the focus position of -3mm focus and -4mm focus. As the focus moved toward the inside of the material more deeply, the exit diameter would decrease. The diameter of entrance and exit would increase in pore size as the processing time increased, and then reached saturation. The use of femtosecond laser filament processing has begun to bear fruit.. But it still needed further improvement. It could be seen that the millimeter-scale deep micropores processed by the femtosecond laser was a feasible processing method.

Acknowledgments

References

1. Naslain R. Design, preparation and properties of non-oxide CMCs for application in engines and nuclear reactors: An overview. Composites Science and Technology 2004; 64(2): 155–170.

2. Zhang L, Cheng L. Discussion on strategies of sustainable development of continuous fiber reinforced ceramic matrix composites. Acta Materiae Compositae Sinica 2007; 2: 000.

3. Hasegawa A, Kohyama A, Jones RH. Critical issues and current status of SiC/SiC composites for fusion. Journal of Nuclear Materials 2000; 283: 128–137.

4. Mcnally CA, Folkes J, Pashby IR. Laser drilling of cooling holes in aeroengines: State of the art and future challenges. Materials Science and Technology 2004; 20(7): 805–813.

5. Fan Z, Dong X, Wang K, *et al*. Effect of drilling allowance on TBC delamination, spatter and re-melted cracks characteristics in laser drilling of TBC coated superalloys. International Journal of Machine Tools & Manufacture 2016; 106: 1–10.

6. Zhai Z, Wang W, Zhao J, *et al*. Influence of surface morphology on processing of C/SiC composites via femtosecond laser. Composites Part A: Applied Science & Manufacturing 2017; 102: 117–125.

7. Fan Z, Wang K, Dong X, *et al*. The role of the surface morphology and segmented cracks on the damage forms of laser re-melted thermal barrier coating in presence of a molten salt ($Na_2SO_4+V_2O_5$), Corrosion Science 2017; 115: 56–67.

8. Fan Z, Wang K, Dong X, *et al*. Evaluation of microstructural evolution and corrosion types in ultrasonic assisted laser re-melted thermal barrier coatings under exposure to molten salts, Materials Letters 2017; 188: 145–148.

9. Zhang J, Cui J, Wang X, *et al*. Recent process in the preparation of horizontally ordered carbon nanotube assemblies from solution. Physica Status Solidi A: Applications and Materials Science 2018; 215(6): 1700719.

10. Pan A, Wang W, Mei X, *et al*. Fractal titanium oxide under inverse 10-ns laser deposition in air and water. Applied Physics A 2017; 123(4): 253.

11. Cui J, Yang L, Wang Y, *et al*. Nanospot Soldering Polystyrene Nanoparticles with Optical Fiber Probe Laser Irradiating Metallic AFM Probe based on Near-Field Enhancement Effect, ACS Applied Materials & Interfaces 2015; 7(4): 2294–2300.

12. He F, Cheng Y, Xu Z, *et al*. Direct fabrication of homogeneous microfluidic channels embedded in fused silica using a femtosecond laser. Optics Letters 2010; 35(3): 282–284.

13. Fan Z, Wang K, Dong X, *et al*. Influence of columnar grain microstructure on thermal shock resistance of laser re-melted ZrO2-7 wt.% Y_2O_3 coatings and their failure mechanism. Surface & Coatings Technology 2015; 277: 188–196.

14. You Y, Dong Y, Li X, *et al*. An experimental investigation of the effects of femtosecond laser helical drilling: Influence of process parameters 2017; 265(1): 012014.

15. Hu Y, Nie J, Ye Q, *et al*. Femtosecond laser filamentation with different atmospheric pressure gradients. Optik - International Journal for Light and Electron Optics 2016; 127(23): 11529–11533.

16. Hao ZQ, Zhang J, Xi TT, *et al*. Optimization of multiple filamentation of femtosecond laser pulses in air using a pinhole. Optics Express 2007; 15(24): 16102–16109.

17. Sun X, Xu S, Zhao J, *et al*. Impressive laser intensity increase at the trailing stage of femtosecond laser filamentation in air. Optics Express 2012; 20(4): 4790–4795.

18. Liu B, Wang W, Jiang G, *et al*. Study on hierarchical structured PDMS for surface super-hydrophobicity using imprinting with ultrafast laser structured models. Applied Surface Science 2016; 364: 528–538.

19. Liu B, Jiang G, Wang W, *et al*. Porous microstructures induced by picosecond laser scanning irradiation on stainless steel surface. Optics and Lasers in Engineering 2016; 78: 55–63.

20. Xu G, Dai Y, Cui J, *et al*. Simulation and experimental of femtosecond laser polishing quartz material. Integrated Ferroelectrics 2017; 181, 60–69.

21. Ito Y, Shinomoto R, Nagato K, *et al*. Mechanisms of damage formation in glass in the process of femtosecond laser drilling [J]. Applied Physics A 2018; 124(2): 181.

22. Corman G, Upadhyay R, Sinha S, *et al*. General Electric Company: Selected Applications of Ceramics and Composite Materials. Materials Research for Manufacturing. Springer International Publishing 2016; 59–91.

23. Grudtsyn YV, Koribut AV, Trofimov VA, *et al*. Femtosecond pulse self-shortening in Kerr media due to transient regime of multiple filamentation. Journal of the Optical Society of America B 2018; 35(5): 1054–1058.